Colloids and Surfaces B: Biointerfaces 240 (2024) 113968

Contents lists available at ScienceDirect

Colloids and Surfaces B: Biointerfaces

journal homepage: www.elsevier.com/locate/colsurfb

Photothermal therapy of xenografted tumor by carbon nanoparticles-Fe (II) complex

Zehui Gou [a], Kexin Tang [b], Cheng Zeng [b], Huahui Yuan [b], Chun Zhang [b], Yuanfang Huang [b], Ting Qu [b], Qian Xin [b], Yufeng Zhao [b], Guangfu Zeng [b], Jinmei Yang [b], Ping Xie [c], Sheng-Tao Yang [d,*], Xiaohai Tang [b,*]

[a] Department of Medical Ultrasound, West China Hospital/West China School of Medicine, Sichuan University, Chengdu, China
[b] Sichuan Enray Pharmaceutical Sciences Company, Chengdu, China
[c] State Key Laboratory of Oral Diseases, West China, College of Stomatology, Sichuan University, Chengdu, China
[d] Key Laboratory of Pollution Control Chemistry and Environmental Functional Materials for Qinghai-Tibet Plateau of the National Ethnic Affairs Commission, School of Chemistry and Environment, Southwest Minzu University, Chengdu 610041, China

ARTICLE INFO

Keywords:
Carbon nanoparticles-Fe(II) complex
Photothermal therapy
Reactive oxygen species
Precise temperature control
Toxicity

ABSTRACT

Due to the unique structure, carbon nanomaterials could convert near-infrared (NIR) light into heat efficiently in tumor ablation using photothermal therapy (PTT). However, none of them has been applied in clinical treatment, because they have not been approved for clinical evaluations and the precise temperature control facility is scarce. In this study, we designed a temperature-responsive controller for PTT and used carbon nanoparticles-Fe (II) complex (CNSI-Fe) as photothermal conversion agent (PTA) for PTT of tumor in vitro and in vivo. CNSI-Fe was an innovative drug under the evaluations in clinical trials. CNSI-Fe showed excellent photothermal conversion ability in water to increase the water temperature by 40 °C within 5 min under irradiation of 808 nm laser at 0.5 W/cm^2. The temperature was precisely controlled at 52 °C for both in vitro and in vivo tumor inhibition. CNSI-Fe with NIR irradiation showed higher tumor cell inhibition than CNSI. In tumor bearing mice, CNSI-Fe with NIR irradiation achieved an inhibition rate of 84.7 % and 71.4 % of them were completely cured. Mechanistically, CNSI-Fe under NIR irradiation induced the radical generation, oxidative damage and ferroptosis to kill tumor. In addition, CNSI-Fe showed good biosafety during PTT according to hematological, serum biological and histopathological examinations. These results indicated that the combination of chemotherapy and PTT provided higher antitumor efficiency using CNSI-Fe as PTA.

1. Introduction

Photothermal therapy (PTT) of tumor is a widely studied approach to kill cancer cells by converting the light into heat through the help of photothermal conversion agents (PTAs) [1,2]. PTT is a noninvasive treatment with minimal side effects and high specificity. Typically, PTAs accumulate in tumor by targeting moieties, enhanced permeability and retention (EPR) effects or direct intratumoral injection [3]. When light irradiates on tumor site, PTAs absorb the light to generate heat and increase the temperature of tumor tissue, which leads to the ablation of tumor [4]. An excellent PTA requires a large absorption cross-section, high photothermal conversion efficiency, high stability and low toxicity [1,2]. Diverse species have been developed for PTT applications, including organic materials [5], polymers [6], inorganic nanomaterials [7], and inorganic-organic hybrids [8].

Precise temperature control is a crucial issue for PTT [9]. During PTT, the tumor cells were ablated by NIR light generated heat. If the tumor temperature is too low, there might be tumor cells surviving, which would inevitably lead to the metastasis and recurrence of tumor [10]. On the other hand, if the temperature goes too high and heterogenous, PTT might induce damage to surrounding normal tissues [10]. In addition, at 60 ℃ and higher, the tumor antigen would be destroyed to inhibit the beneficial immunoreaction [11,12]. Therefore, during the research and development (R&D) of PTT, the near infrared (NIR) irradiation equipment with precise temperature control function is highly desired.

Among the novel PTAs, nanomaterials are a category of promising ones that have small sizes and designable surficial functionalities. CuS

* Corresponding authors.
E-mail addresses: yangst@swun.edu.cn (S.-T. Yang), pharmmateceo@enraypharm.com (X. Tang).

https://doi.org/10.1016/j.colsurfb.2024.113968
Received 18 March 2024; Received in revised form 3 May 2024; Accepted 11 May 2024
Available online 13 May 2024

nanoparticles (NPs) could target the nuclei after the functionalization of arginine-glycine-aspartic acid (RGD), which inhibited the growth and recurrence of HeLa tumor in PTT [13]. Gold nanorods coated with silica was useful for NIR-II photothermal ablation of hepatocellular carcinoma, and the PTT could be combined with programmed death-ligand 1/ vascular endothelial growth factor (PD-L1/VEGF) blockade therapy [14]. Degradable phthalocyanine nano-assembly (nanoPcDA$_2$) accumulated in tumor after intravenous injection to inhibit 92 % of tumor growth at 300 J/cm^2 [15]. Chang et al. used gold modified Ti_3C_2-Mxene nanocomplex for PTT [16]. After the photothermal induced death of immunogenic cells, and accelerate the mature of dendritic cells (DC) and the infiltration of tumor by T cells. With the immunological therapy of OX40 antibody, this method showed good efficiency in treating 4T1 tumor [16]. Zhao et al. coted carbon nanotubes with peptide lipid (PL) and sucrose laurate (SL) to build a temperature-sensitive and photothermal active delivery system of siRNA, which could inhibit the tumor growth [17]. Despite the great achievements of nano-PTAs, they have not been applied in clinical treatments. In particular, the safety concerns of nanomaterials hinder the clinical applications of nano PTAs.

Carbon nanomaterials with proper surface functionalization usually have very good biosafety, such as graphene, carbon nanotubes (CNTs), and carbon quantum dots (CQDs). The sp^2 carbon structure of carbon nanomaterials has good NIR absorption and high photothermal conversion efficiency. Thus, these carbon nanomaterials find great potentials in PTT. For example, ultrasmall graphene oxide (GO) was fabricated with poly(dopamine) for PTT and drug delivery of doxorubicin [18]. The tumor temperature increased to 50 °C within 120 s under laser irradiation and the tumor growth was largely completed. CNTs were functionalized by thyroid hormone stimulating receptor antibody for papillary thyroid cancer tumor therapy [19]. CNTs accumulated in tumor and increased the tumor temperature for 33 °C to achieve efficient tumor growth inhibition. N-doped CQDs could be swallowed by cancer cells for two-photon fluorescence-guided precise photothermal therapy [20]. Ultrasmall iron embedded in mesoporous carbon nanoparticle (C/Fe NPs) could be applied in for hydrogen (H_2) assisted photothermal synergistic therapy of H22 hepatic tumor [21]. The major problem of carbon nanomaterials is their heterogeneous nature, which make the commercial production of carbon nanomaterials with uniform properties among batches is very difficult.

To accelerate the clinical applications of nano-PTAs, using currently clinical approved nanomaterials or those under evaluation of clinical trials is preferred. Carbon nanoparticle suspension injection (CNSI, also known as Canarine) is the only clinically approved carbon nanomaterial for tumor drainage lymph node staining [22,23]. Previously, we found that CNSI absorbed light in a wide range and convert the light into energy efficiently [24]. Under NIR irradiation, CNSI could generate enough heat to kill cancer cells in vitro and in vivo. After the treatment, the recurrence of tumor was largely avoided. More importantly, when CNSI was complexed with Fe^{2+}, the CNSI-Fe complex could serve as chemotherapy drug to inhibit the tumor growth. CNSI-Fe was approved for clinical trials and the phase I trial is currently undergoing. The literature has suggested that the combination of chemotherapy and PTT holds great potential and better therapeutic effect [25]. For CNSI-Fe, it is worthwhile to evaluate its performance in PTT. CNSI-Fe has been pilot-scale produced to meet the clinical trials' requirements. The good biosafety of CNSI-Fe has been proven in the clinical trial I. These two advantages of CNSI-Fe would definitely accelerate the applications of PTT in clinical uses.

In this study, we adopted CNSI-Fe as the photothermal converting reagent for tumor therapy. A PTT facility with precise temperature control was designed for this study (Scheme S1). The photothermal conversion ability of CNSI-Fe was measured in solution. The therapeutic efficiencies were assayed in vitro and in vivo at different temperatures. The therapeutic mechanisms of CNSI-Fe were investigated by hydroxyl radicals, oxidative stress, Fe uptake, and immunohistochemistry. The biosafety of CNSI-Fe during PTT was evaluated by serum biochemistry, hematology and histopathology. CNSI-Fe was directly compared with CNSI during the in vitro and in vivo evaluations to highlight the importance of Fe(II). The implications to the clinical applications of CNSI-Fe in the PTT of tumor are discussed.

2. Materials and methods

2.1. Preparation of CNSI-Fe

CNSI-Fe was consisted by two major components, CNSI and Fe(II). To prepare CNSI, poloxamer 400 mg was dissolved in 20 mL of water and then added with 1.0 g of C40 powder (Mitsubishi Chemical Co., Tokyo, Japan). The mixture was homogenized for 5 min and treated by an ultrahigh pressure homogenizer at 20,000 psi for 3 times to obtain black suspension. To the suspension, $FeSO_4{\cdot}H_2O$ was added at designed concentration before use. The CNSI-Fe samples were characterized by transmission electron microscope (TEM, Thermo Scientific, Talos F200S G2, USA), dynamic light scattering (DLS, Zetasizer Nano ZS90, Malvern Instruments, Malvern, UK), Fourier transform infrared spectroscopy (FTIR, Thermo Scientific Is50, USA), Raman spectroscopy (Horiba Scientific LabRAM HR Evolution, France) and X-ray photoelectron spectroscopy (XPS, Thermo Scientific K-Alpha, USA).

2.2. Photothermal conversion ability of CNSI-Fe

The CNSI-Fe was directly compared with CNSI at different C-equivalent concentrations (0–667 μg/mL). The samples were placed in glass dishes (1.0 mL/dish) and irradiated under NIR laser (808 nm, CW laser) at 0.5 W/cm^2 for 10 minutes. The temperature changes before and after irradiation were recorded by a thermometer (opSens, Tempsens Instrument Pvt. Ltd., Québec, Canada). Separately, CNSI-Fe and CNSI at a C-equivalent concentration of 333 μg/mL were irradiated at 0.5, 1.0 and 2.0 0.5 W/cm^2 for 10 min to investigate the influence of irradiation power. The photothermal conversion efficiency of CNSI-Fe was measured following literature protocol [26].

2.3. Hyperthermia of tumor cells in vitro

CT26.WT cells were cultured in 6-well plates at a density of 1×10^5 cells/mL following standard protocols. After 24 h, the culture medium was discharged and supplemented with culture medium containing CNSI-Fe (333:100 μg/mL, C:Fe), CNSI or none. After another 24 h, the wells of NIR group, CNSI + NIR group, and CNSI-Fe + NIR group were irradiated by 808 nm laser at initial power density of 0.5 W/cm^2 for 5 min. The power density was automatically controlled by the temperature responsive power control system to maintain the temperature at set values. During the irradiation, the irradiation power was automatically adjusted to maintain the temperature at 42–52 °C. For the control group, CNSI group and CNSI-Fe group, no irradiation was applied. The cells were cultured for another 48 h. The cells were digested with trypsin for counting and cell proliferation rates were calculated accordingly. The combination effects of PTT and chemotherapy were examined by Eq. 1, where $q > 1$ means synergistic, $q = 1$ means additive, and $q<1$ means antagonistic. In equation 1, E_A refers to the effect of PTT (CNSI + NIR), E_B refers to chemotherapy (CNSI-Fe), and E_{A+B} refers to the combination of PTT and chemotherapy (CNSI-Fe + NIR).

$$q = E_{A+B}/(E_A + E_B\text{-}E_A \times E_B) \quad (1)$$

To investigate the therapeutic mechanisms, cells from the control group, CNSI-Fe group, CNSI + NIR group and CNSI-Fe + NIR groups were collected after the treatment. To measure the hydroxyl radicals, the cells were freeze thawing and added with 5,5-dimethyl-1-pyrroline-N-oxide (DMPO) for electron spin resonance (ESR) analyses (JES-FA200, JEOL, Japan). To measure the Fe contents, the cells were digested with 5 mL of HNO_3 in a microwave digestion instrument at 180 °C for 30 min.

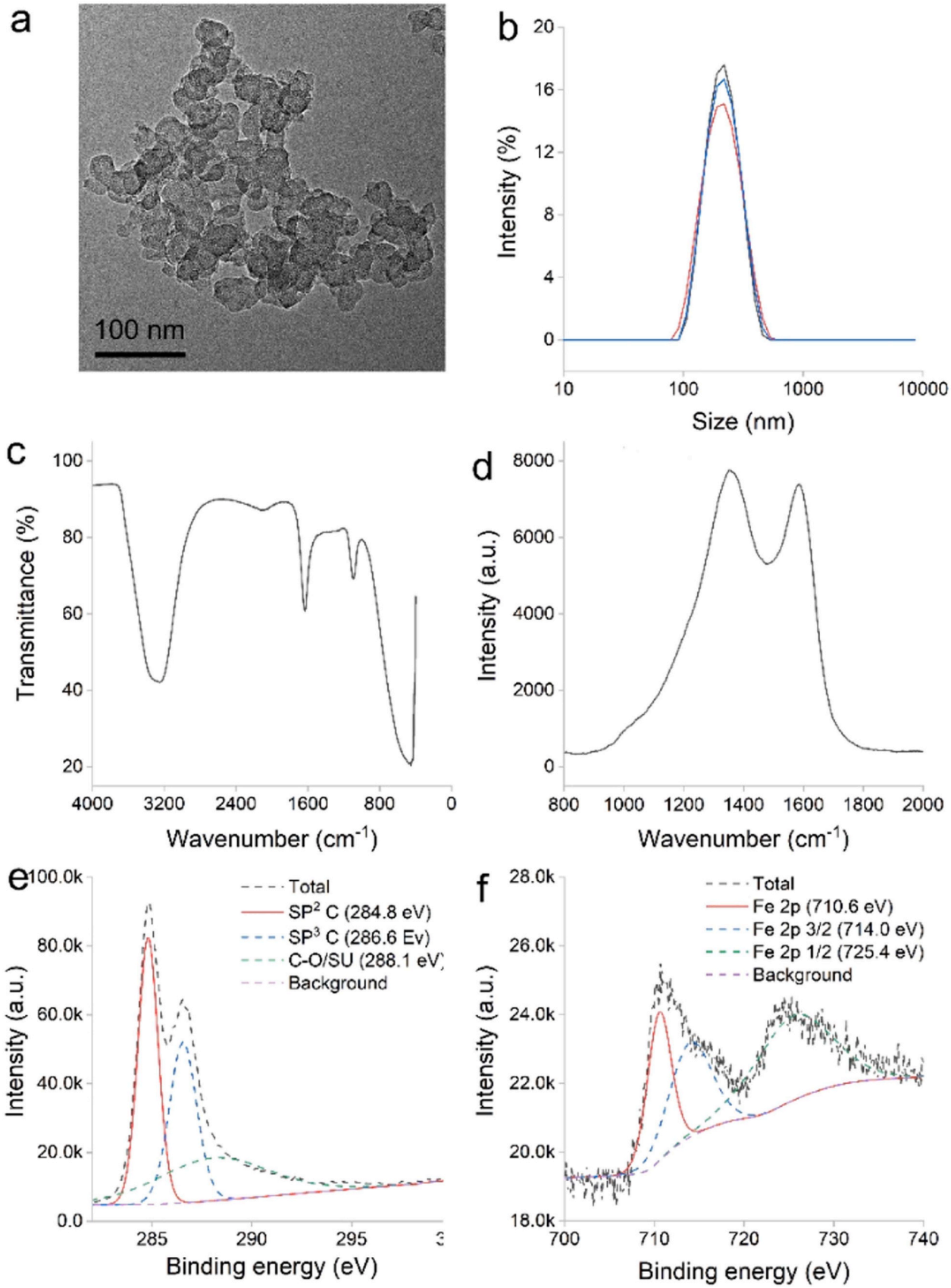

Fig. 1. Characterization data of CNSI-Fe complex. (a) TEM image; (b) DLS spectra; (c) FTIR spectrum; (d) Raman spectrum; (e) C1s XPS spectrum; (f) Fe2p XPS spectrum.

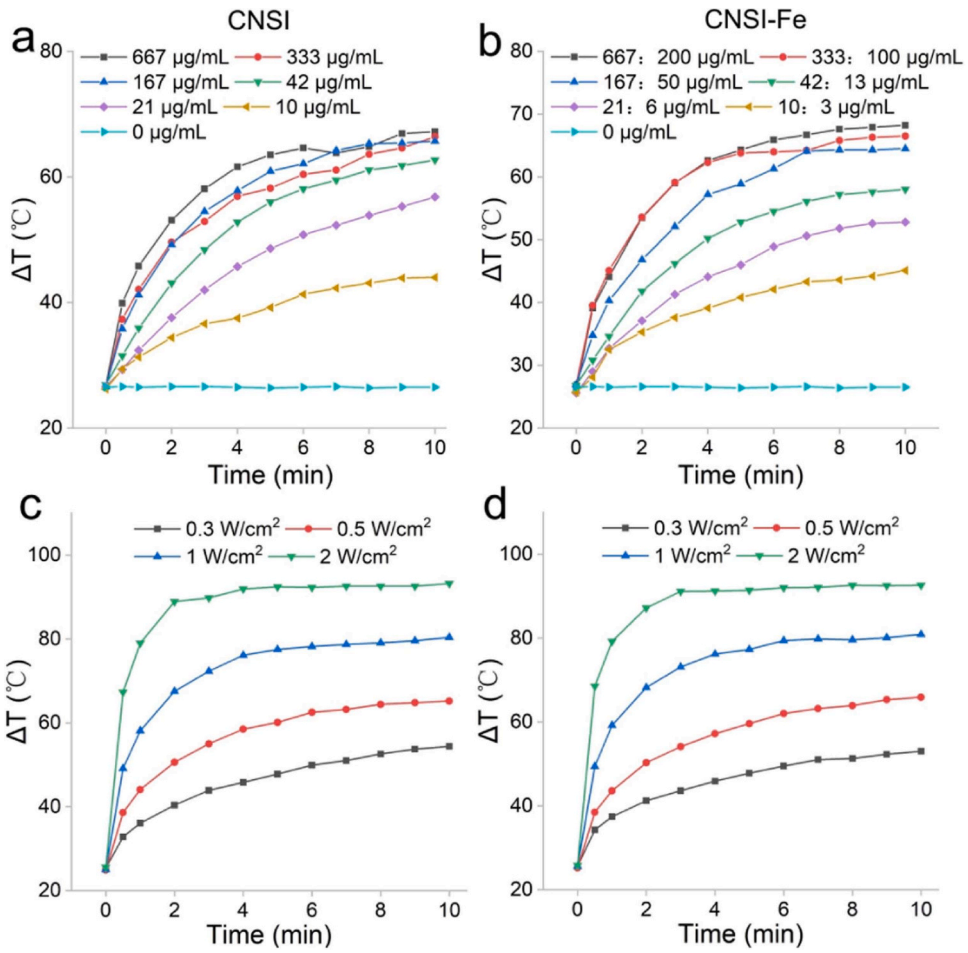

Fig. 2. Representative plots for in vitro heating experiments with CNSI (left) and CNSI-Fe (right). (a, b) concentration-dependent heating; (c, d) irradiation power density-dependent heating.

The Fe concentrations of the digestion solutions was quantified by inductively coupled plasma-mass spectrometry (ICP-MS, 7700X, Agilent, USA). The oxidative stress parameters, including H_2O_2, peroxidase (POD), glutathione (GSH) and malondialdehyde (MDA), were measured using commercial kits following the recommended protocols (Beijing Solarbio Biotechnology Co., LTD.).

2.4. Inhibition of xenografted tumor in vivo

The animal experiments were approved by the Ethics Committee of Southwest Minzu University and performed in compliance with the Animal Care and Use Program Guidelines of the Sichuan Province, China. Animals were raised in plastic cages and kept on a 12-hour light/dark cycle. Food and water were available *ad libitum*. Following acclimation, the mice were inoculated by the injection of 0.1 mL CT26.WT cell suspension (3×10^7 cells) on the right limb. After 7 d, the tumor volumes reached 100–150 mm^3 and they were randomly divided into six groups (7 mice for each), namely, control group, CNSI group, CNSI-Fe group, NIR group, CNSI + NIR group, and CNSI-Fe + NIR group. The mice were intratumorally injected with 50 μL of saline, CNSI or CNSI-Fe, respectively. The second injection was applied at 7 d post the first injection. After each administration for 2 h, the mice were irradiated by 808 nm laser for 10 min at a designed temperature of 52 °C for NIR group, CNSI + NIR group and CNSI-Fe + NIR group. The temperature was monitored by the infrared (IR) thermal imager. The tumor size and bodyweight were recorded with intervals of 2 d. The mice were sacrificed at 14 d. For mechanism investigations, the tumor tissues were collected for caspase 3 measurements. For hematoxylin-eosin staining (HE). The tissues were dissected (tumor, liver, spleen, lung, and kidneys), fixed with 10 % formaldehyde, sampled following the standard protocol of HE and imaged (Eclipse ci, Nikon, Tokyo, Japan). For TUNEL assay, the tumor tissues were collected for terminal deoxynucleotidyl transferase-mediated dUTP nick-end-labeling (TUNEL) staining by Wuhan Servicebio Technology Co. following standard protocols. The serum biochemistry and hematological parameters were measured following our previous protocols [25]. In another set of experiments, the mice were observed for 3 months to calculate the survival rates.

2.5. Statistical analysis

All data were expressed as the mean with the standard deviation (mean ± SD). Differences were considered significant at $p < 0.05$ according to the results of Student's-t test.

3. Results and discussion

3.1. Characterization of CNSI-Fe

CNSI-Fe was composed by carbon NPs and Fe^{2+} in the presence of suspension reagent poloxamer. The composition of CNSI in this study was different from our previous study [24], because poloxamer allowed better dispersion than polyvinyl pyrrolidone (PVP) during the sterilization. Under TEM, it could be recognized that the carbon NPs had diameters around 25 nm (Fig. 1). The carbon NPs obviously would aggregate due to the π-π interaction and hydrophobic interaction, which was reflected by the hydrodynamic radii of 196.1 ± 1.6 nm during the

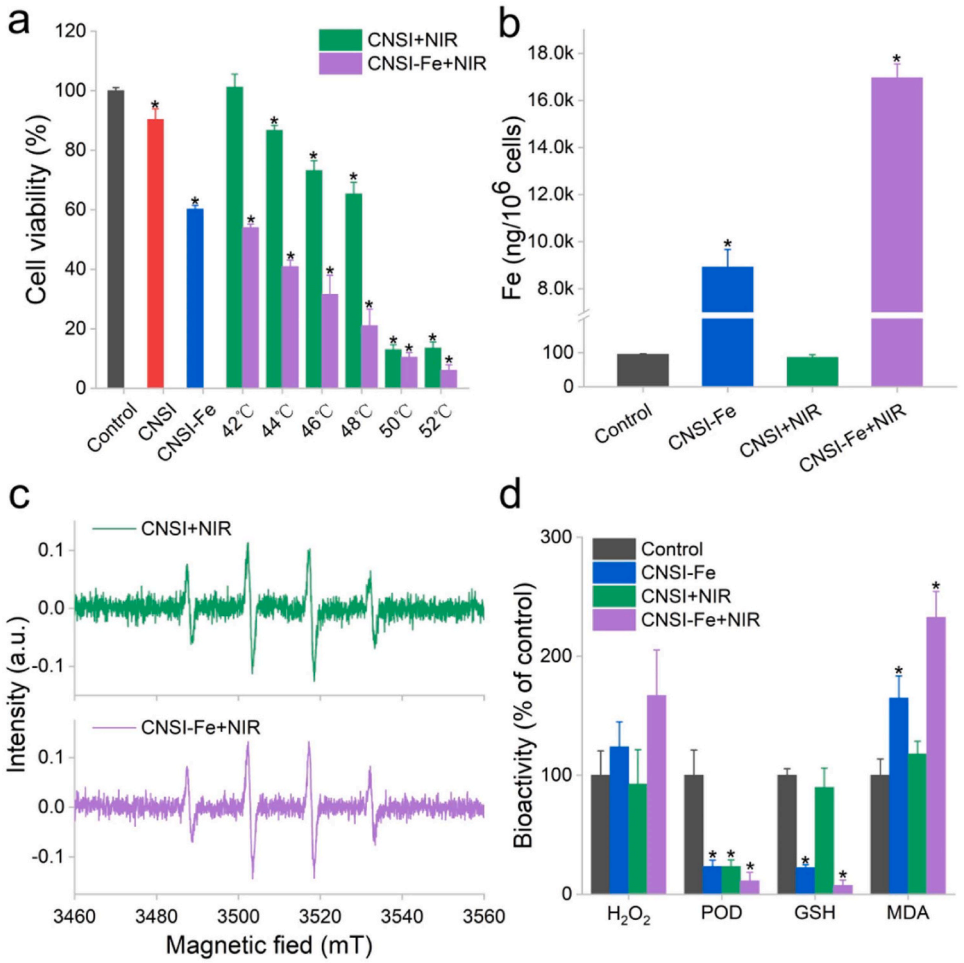

Fig. 3. Inhibition of CT26.WT cells in vitro by CNSI-Fe assisted PTT. (a) cell proliferation; (b) Fe uptakes; (c) generation of ·OH radical; (d) oxidative stress.

DLS measurements. It was consistent with the TEM observation that nearly no single carbon NPs were found. The IR spectrum identified the signals from both carbon NPs and also poloxamer, including 3260 cm^{-1} for -OH, 1100 cm^{-1} for C-O, 1640 cm^{-1} for C═C. The typical graphite structure in carbon NPs was evidenced by Raman spectrum. The G-band was found at 1590 cm^{-1} and the D-band was presented at 1350 cm^{-1}. The graphite structure was the main reason of NIR absorption, which was also widely observed in carbon nanotubes and graphene materials [27–29]. According to the XPS analyses, the carbon atoms were in forms of C-C (37.0 %), C-O (30.3 %), C═O (32.7 %). The presence of Fe^{2+} was evidenced by the Fe2p XPS spectrum. The best of CNSI-Fe is that the commercial production of CNSI-Fe has been achieved for clinical trials. Now, CNSI-Fe could be produced at a scale of kilograms, equaling to 20,000 packages.

3.2. Photothermal conversion in solution by CNSI-Fe

The photothermal conversion capability of CNSI-Fe was measured by monitoring the temperature increases of CNSI-Fe dispersion under NIR irradiation. During the 10-minute irradiation at 0.5 W/cm^2, the blank solution showed very small temperature increases of 26.4–26.6 °C (Fig. 2a). The temperature increases depended on the carbon NP concentrations, where 10 μg/mL of carbon led to much faster temperature increases for both CNSI and CNSI-Fe groups. The temperature reached a plateau after 5 min and the differences were small among 167–667 μg/mL groups. At carbon equivalent concentration of 167 μg/mL and higher, the NIR light was already fully absorbed, thus the temperature increases were similar (63.5 °C in the CNSI group vs 64.3 °C in the CNSI-Fe group at the carbon equivalent concentration of 667 μg/mL). It should also be noted that adding Fe^{2+} into CNSI did not affect the efficiency of PTA. The temperature increases of CNSI-Fe groups were 98 % ± 4 % of those of CNSI groups at all concentrations. The temperature similar increases should be attributed to the nearly same photothermal conversion efficiencies of CNSI-Fe (50.9 %) and CNSI (49.5 %). The photothermal conversion efficiency of CNSI-Fe was comparable to other high-performance nano-PTA. For example, GO/hydroxyapatite composite had a photothermal conversion efficiency of 22.2 % [26]. Fe_3O_4 NPs showed a photothermal conversion efficiency of 49.14 % [30]. The values were 59.85 % forγ- Fe_2O_3 and 43.3 % for $FePS_3$ nanosheets [31,32]. In another set of experiments, we investigated the influence of irradiation power density using carbon-equivalent concentration of 333 μg/mL (Fig. 2b). At 2 W/cm^2, the final temperature increases of CNSI-Fe group reached 92.6 °C, and the value was 93.2 °C for CNSI group. CNSI-Fe obviously had high photothermal conversion capability that was competitive to other carbon nanomaterials, e.g. carbon nanotubes, graphene quantum dots, Fe_3O_4 modified graphene [33,34]. The retained photothermal conversion performance of CNSI-Fe upon the supplement of Fe^{2+} allow the combined PTT and chemotherapy applications for tumor inhibition.

3.3. Photothermal therapy in vitro

The therapeutic effect of CNSI-Fe in PTT was measured by counting the cell proliferation changes of CT26.WT cells (Fig. 3a). The cell temperature was precisely controlled through the temperature responsive power control system. Consistent with our previous observations, CNSI-

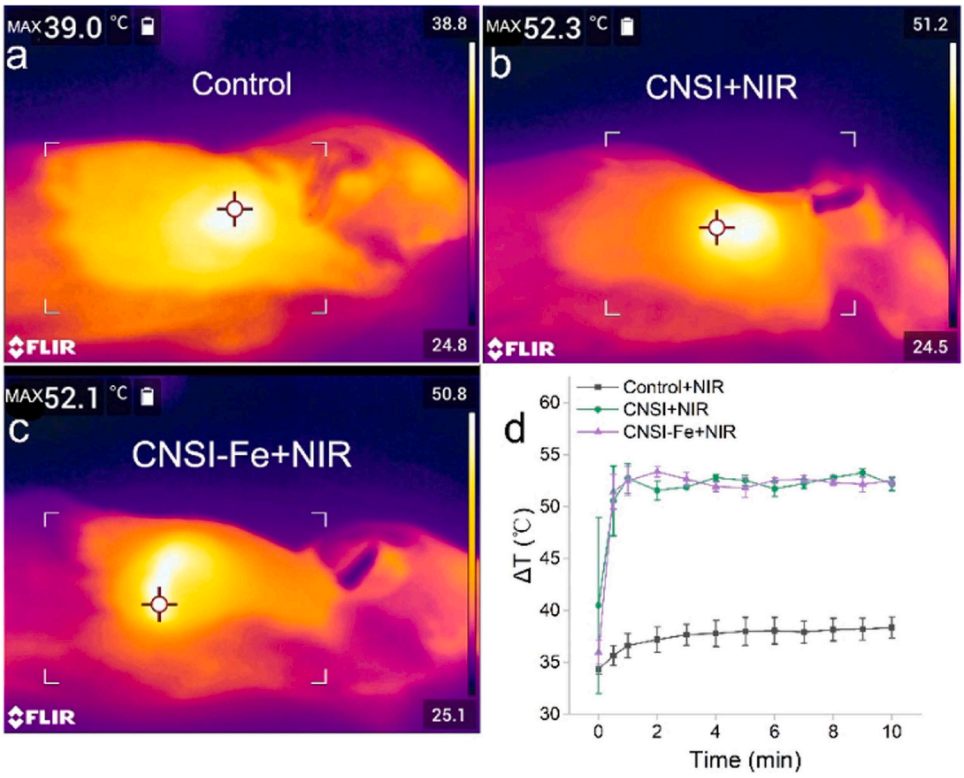

Fig. 4. IR thermal images of CT26.WT tumor bearing mice under NIR irradiation. (a–c) IR thermal images; (d) tumor temperature changes.

Fe could partially kill CT26.WT cells without NIR irradiation (48.5 % of the control), but CNSI alone was nontoxic. Under NIR irradiation, we could precisely control the temperature by our homemade facility. At 50 °C and higher, there were no significant difference between CNSI-Fe + NIR groups and CNSI + NIR groups. The photothermal conversion ability should be attributed to CNSI rather than Fe^{2+} or other components, because without CNSI the PTA performance was ignorable (Fig. S1). All had cell proliferation rates of less than 1 % of the control. Meaningful results were presented at 42–48 °C, where CNSI-Fe + NIR groups were statistically better than CNSI + NIR groups. At 46 °C, the q value was larger than 1 ($q = 1.22$), indicating the combination effect of PTT from CNSI and chemotherapy from Fe^{2+}.

To investigate the therapeutic mechanisms, we firstly measured the Fe contents in CT26.WT cells. The control group had a Fe content of 95.1 ±2.9 ng/10^6 cells, which was not affected by CNSI during PTT (86.3 ±9.8 ng/10^6 cells). CNSI-Fe could largely increase the cellular Fe content to 8926.7 ± 914.9 ng/10^6 cells. PTT destroyed the cellular structure, resulting in even higher Fe content of 16,958.0 ± 728.5 ng/10^6 cells. In literature, NIR light significantly promoted cell uptake of drug compared to those without irradiation, resulting in an enhanced intracellular drug accumulation. Such examples were gold nanoshell-coated betulinic acid liposomes, low-molecular-weight hyaluronic acid/chitosan nanocomplexes and size-switchable albumin nanocluster [35–37]. High temperature would lead to the protein denaturation to affect the enzyme and structure proteins. This directly contributed to the cell death and higher temperature resulted in more cell deaths (Fig. 3a). Another widely accepted mechanism of PTT is the generation of radicals to attack the tumor cells. Hydroxyl radicals were identified in CNSI + NIR group, which was slightly increased in CNSI-Fe + NIR group. It should be noted that CNSI-Fe alone could generate hydroxyl radicals, too (Fig. S2). The radicals would inevitably lead to oxidative stress in cells. CNSI + NIR group induced the mildest oxidative stress in CT26.WT cells. Only the POD level significantly reduced for CNSI + NIR group. CNSI-Fe group induced the increase of H_2O_2 and MDA, and led to the decreases of POD and GSH. The oxidative damage was most serious in CNSI-Fe + NIR group. All parameter changes were more than the other two groups, which could explain the better therapeutic effect. In our view, the Fe accumulation, high temperature, radical generation and ferroptosis contributed to the therapeutic effects.

3.4. Photothermal therapy in vivo

The in vivo tumor ablation was highly dependent on the tumor temperature. Using our homemade facility, the temperature could be well controlled during the ablation. The IR thermal imager recorded the temperature of the tumor sites (Fig. 4). The NIR irradiation during our evaluation only increased the temperature of tumor site to 39 °C. Using CNSI and CNSI-Fe as PTAs, the rapid increases of tumor temperature were achieved within the first 0.5 min. The temperature kept steadily around 52 °C during PTT through our temperature responsive power control system (Fig. 4d). This phenomenon indicated that our facility could control the temperature of tumor site accurately for the following therapeutic evaluations.

The in vivo tumor ablation was performed after intratumoral injection of CNSI-Fe followed by the NIR irradiation. Intratumoral injection was the designed dosing method for CNSI-Fe, which was approved by Center for Drug Evaluation (CDE) for clinical trials. The in vivo tumor ablation was achieved at a tumor site temperature of 52 °C using our homemade facility for CNSI-Fe + NIR group and CNSI + NIR group. Pure NIR irradiation slightly inhibited the tumor growth, but the difference was insignificant (Fig. 5). This was reasonable, because the tumor site temperature was only 39 °C. CNSI did not affect the tumor growth, just as our previous observations[25]. CNSI-Fe without irradiation was very efficient in tumor inhibition (inhibition rate of 64 %), which was through the ferroptosis pathway [25]. Under NIR irradiation, CNSI showed significant inhibition to the tumor growth (77.3 %). In CNSI-Fe + NIR group, the inhibition rate reached 91.9 %, and a combination effect was evidenced ($q = 1.26$). At 14 d, the mice were sacrificed and the tumor tissues were taken out for weighing. The inhibition rates followed the sequence: CNSI-Fe group (64.1 %) < CNSI + NIR

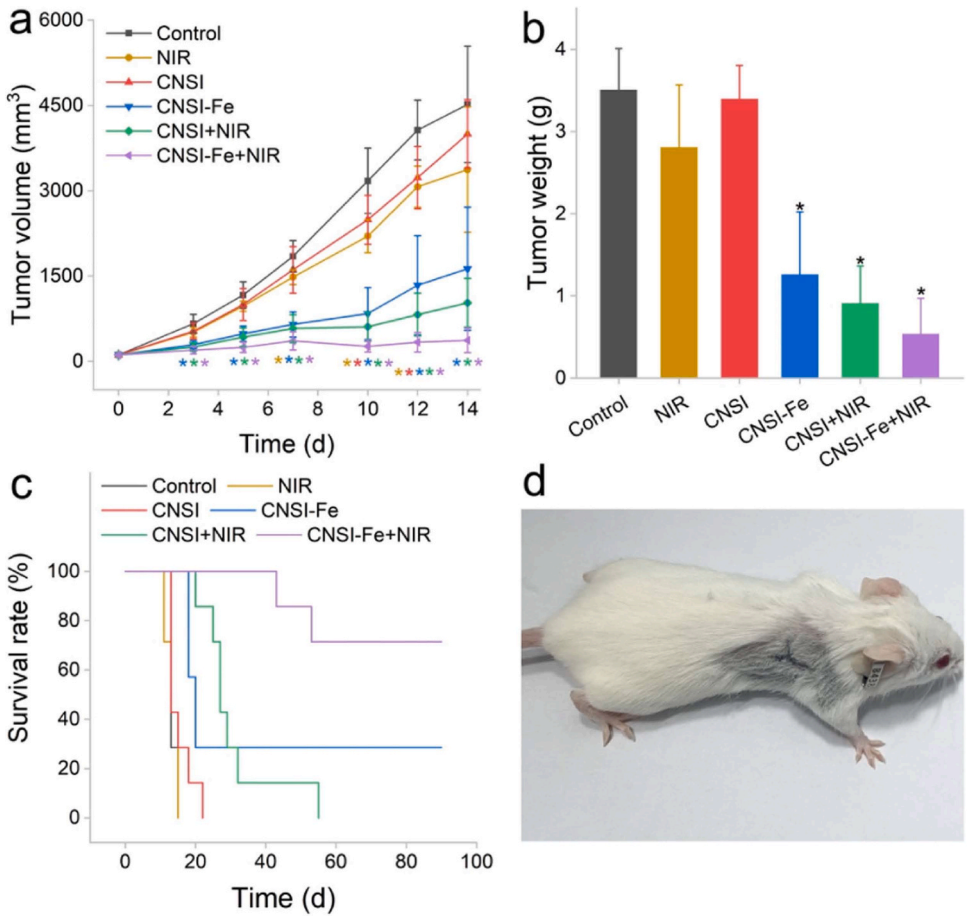

Fig. 5. Tumor ablation by CNSI-Fe under 808 nm laser irradiation. (a) tumor volumes; (b) tumor weights; (c) survival rates; (d) photograph of a presentative mouse after the treating by CNSI-Fe + NIR. The initial power density was 0.5 W/cm^2 and the power density was automatically controlled by the temperature responsive power control system to maintain the temperature at 52 °C for CNSI-Fe + NIR and CNSI + NIR groups.

group (74.1 %) < CNSI-Fe + NIR group (84.7 %). The inhibitions were statistically significant in the three groups, but there was no combination effect. We also collected the tumor tissues for HE staining and TUNEL assay to reflect the therapeutic effects (Fig. S3). All groups showed typical tumor characteristics upon HE staining. Few necrotic cells were found in the control, NIR group and the CNSI groups. Local necrosis occurred in the CNSI + NIR group. CNSI-Fe induced more necrosis, and only CNSI-Fe + NIR group generated massive necrosis. Separate application of CNSI and NIR did not arouse apoptosis according to TUNEL staining. CNSI-Fe resulted most serious apoptosis among all groups, which was well consistent with our previous observations [25]. Coupling with NIR irradiation, the apoptosis level of CNSI-Fe + NIR group decreased comparing to CNSI-Fe group. This might be due to that the heat destroyed the cellular structure too fast to arouse apoptosis. It should be noted that among the 7 mice in each group, some were completely healed. During the survival rate observations, none of CNSI-Fe group was thoroughly cured and all died within two months. CNSI + NIR group had two mice (28.57 %) surviving during the three-month observation period. CNSI-Fe + NIR group had five cured mice (71.43 %). For those cured mice, there was no tumor found after sacrifice. To this regard, although there was no combination effect in tumor weights, the combination of PTT and chemotherapy did increase the survival rates in vivo. Previously, we found that CNSI + NIR could achieve satisfying tumor growth inhibition and prolong the survival period at 53 °C for human thyroid carcinoma tumor. NIR irradiation could extend tumor penetration depth of medicines and help the drug to achieve penetration-enhanced PTT, thereby effectively eliminating tumor cells inside solid tumors [37–39]. The PTT synergically released the carbon monoxide and doxorubicin which effectively eliminate active tumor cells in the periphery of the tumor [38]. Various Fe-based nanomaterials combined with NIR significantly inhibited the growth of implanted tumor xenografts, too [40,41]. Our CNSI-Fe also showed competitive performance to other carbon nanomaterials, such as ultrasmall GO [18], CNTs [19], and C/Fe NPs [21].

The therapeutic mechanisms of CNSI-Fe + NIR group were very similar to the in vitro results. First, the intratumoral injection of CNSI-Fe resulted in largely increase of Fe content (Fig. 6a). Under irradiation, the Fe contents further increased to 30.9 times of the control group and its 17 % higher than that without irradiation. In literature, PTT exhibited high tumor accumulation of a multifunctional Fe-doped polyoxometalate (Fe-POM), which achieved a synergistic PTT/ reactive oxygen species-involved chemodynamic therapy [40]. The overdose of Fe in tumor led to apoptosis as indicated in Fig. 6b. After NIR irradiation, the absolute caspase 3 level was lower than that of CNSI-Fe group without irradiation. This was reasonable because cells died too fast to allow apoptosis. CNSI-Fe + NIR treatment generated hydroxyl radicals in vivo, too (Fig. 6c). The hydroxyl radical signal of CNSI-Fe + NIR group was the strongest comparing to the control, CNSI-Fe and CNSI + NIR groups. The radicals might stimulate the expression of inflammatory cytokines. However, in our pre-evaluations, we did not observe the increase of inflammatory cytokines (data not shown). It might be due to the high temperature that quickly destroyed the cellular structures before the initial of inflammation. Both radicals and high temperature could kill tumor cells, but it is hard to count the contribution portions. In addition, all treatments induced oxidative stress in tumor (Fig. 6d). The hydroxyl radicals were most abundant in

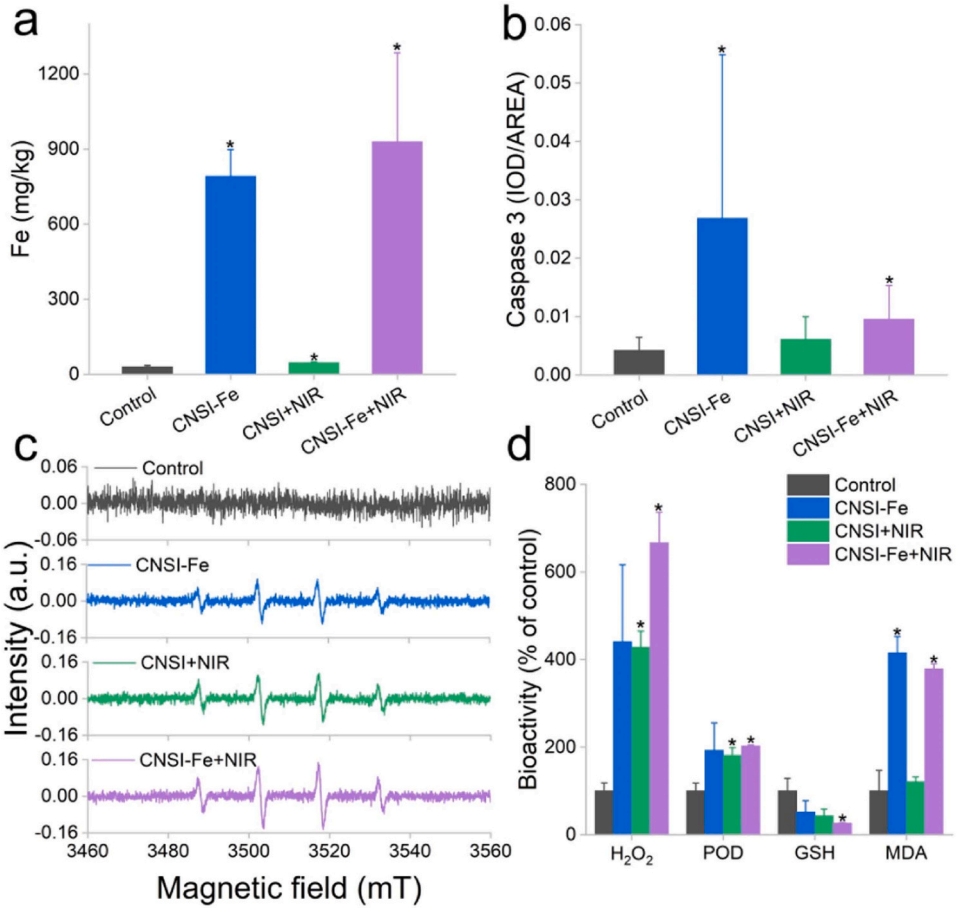

Fig. 6. Mechanism of CNSI-Fe assisted PTT in vivo. (a) Fe accumulation; (b) apoptosis; (c) ·OH radical generation; (d) oxidative stress. * $p < 0.05$ compared with the control.

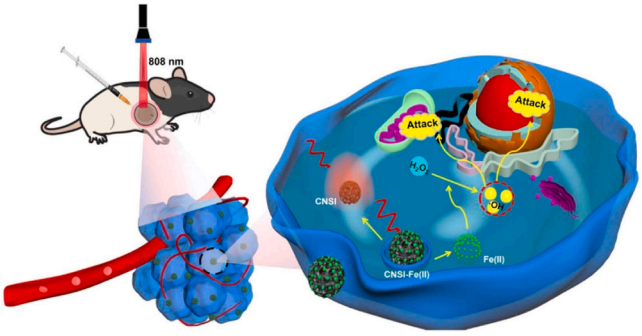

Scheme 1. Cartoon illustration of the therapeutic mechanisms of CNSI-Fe assisted PTT.

CNSI-Fe + NIR group, while CNSI-Fe group and CNSI + NIR group were similar. As another category of ferroptosis indicators, GSH depletion and MDA accumulation were statistically significant in CNSI-Fe + NIR group. Overall, when CNSI-Fe was injected intratumorally, CNSI-Fe retained largely in tumor (Scheme 1). Under irradiation, more Fe^{2+} was trapped by tumor to initiate ferroptosis. The NIR light was absorbed and converted into heat by carbon NPs, which further generate reactive oxygen species to kill tumor cells. The combination of chemotherapy and PTT in our study improved the tumor inhibition and survival rate.

3.5. Biosafety of CNSI-Fe during photothermal therapy

The biosafety of CNSI-Fe has been verified in our previous reports [25]. Its biosafety was also proved by commercial preclinical safety evaluation. More importantly, CNSI-Fe also showed good biosafety in clinical trial I. These facts highlighted the satisfied biosafety of CNSI-Fe for clinical uses. Here, we focused on the biosafety of CNSI-Fe during PTT (Fig. 7). In the hematological analyses, CNSI + NIR group induced the decrease of white blood cell (WBC). This suggested that CNSI + NIR lowered the immune cells and induced a slight immunotoxicity. CNSI + NIR and CNSI-Fe + NIR led to the increase of platelet (PLT). During the chemotherapy of tumor, PLT usually decrease, which is the side effect of chemotherapy [42,43]. CNSI + NIR and CNSI-Fe + NIR increased these parameters, suggesting the good biosafety of NIR to blood circulation. And only CNSI-Fe + NIR group showed statistically significance. The rest were similar to the control group. In the serum biochemical analyses, aspartate aminotransferase (AST) levels decreased in CNSI + NIR group, CNSI-Fe group and CNSI-Fe + NIR group. CNSI-Fe + NIR group also displayed an alkaline phosphata (ALP) increase. The ALP increase should be assigned to the Fe toxicity to hepatic function, considering the increased hepatic Fe accumulations [43,44]. Other parameters kept unchanged comparing to those of control group. In the histopathological examinations, the structure of liver, spleen, lung, kidneys did not change seriously. There were more granulocyte infiltration and lymphocytic infiltration in liver upon NIR irradiation for CNSI + NIR group and CNSI-Fe + NIR group. There was spotty necrosis in liver of CNSI + NIR group and CNSI-Fe + NIR group, too. These observations suggested that CNSI-Fe was of low toxicity to mice during PTT.

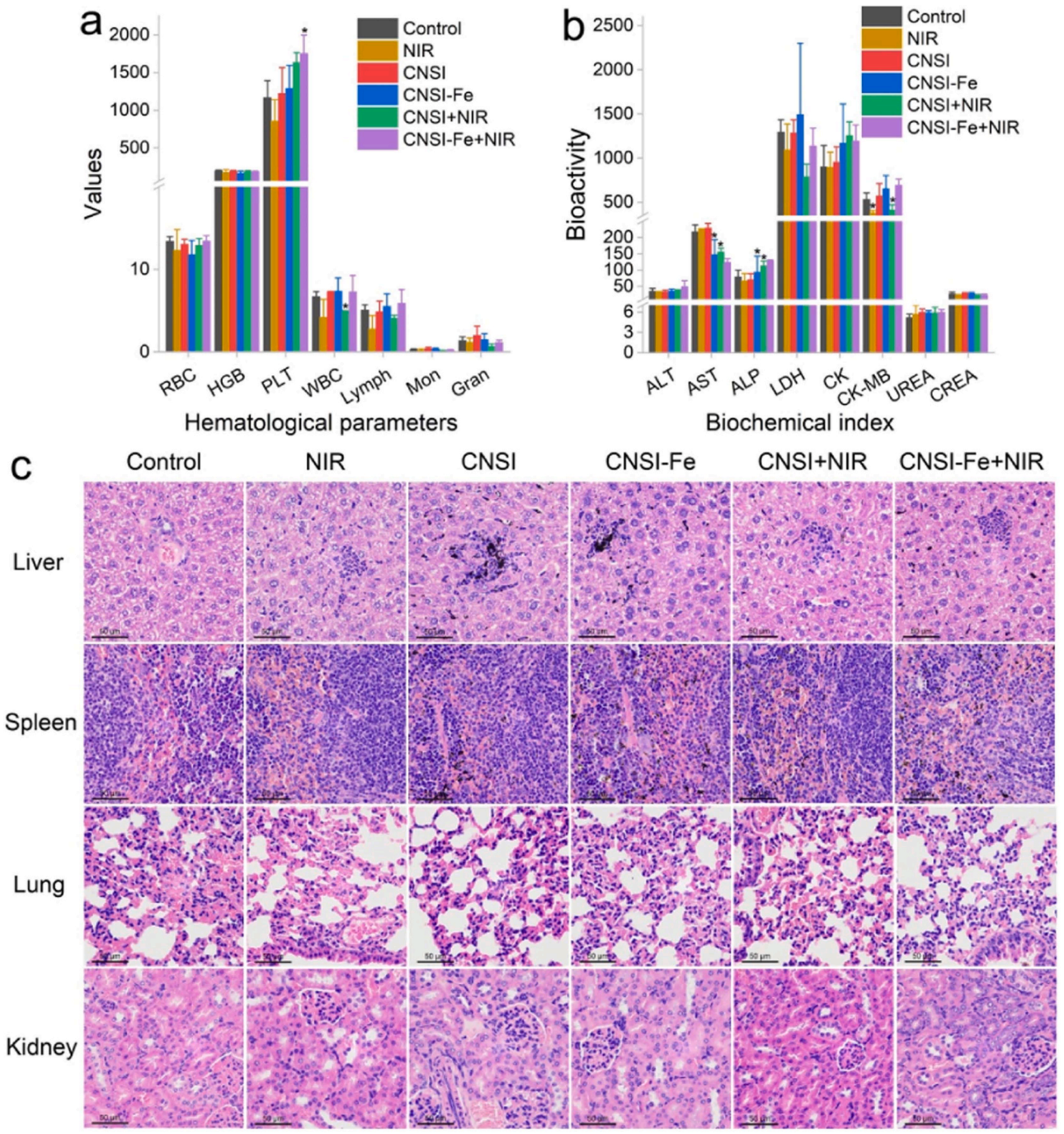

Fig. 7. Biosafety evaluation of CNSI-Fe assisted PTT. (a) hematological parameters; (b) serum biochemistry; (c) histopathological examinations (scale bar = 50 μm). RBC: red blood cell; HGB: hemoglobin; PLT: blood platelet; WBC: white blood cell; Lymph: lymphocyte; Mon: monocyte; Gran: neutrophilic granulocyte; ALT: alanine aminotransferase; AST: aspartate aminotransferase; ALP: alkaline phosphatase; LDH: lactate dehydrogenase; CK: creatine kinase; CK-MB: creatine kinase-MB; CREA: creatinine.

4. Conclusions

In summary, we compared the photothermal conversion ability and therapeutic efficiency of CNSI and CNSI-Fe both in vitro and in vivo, where CNSI-Fe inherited the excellent PTA properties of CNSI and supplemented with the chemotherapy effect of Fe^{2+}. The combination of chemotherapy and PTT allowed higher tumor inhibition rate, prolonged survival period and more cured mice in CNSI-Fe + NIR group. The therapeutic mechanism was associated with radical generation, oxidative damage and ferroptosis. Using homemade facility, we achieved the precise temperature control of tumor site during PTT to avoid unwanted damage to other tissues. In future, CNSI-Fe is hopefully applied in clinical PTT of tumor and stimulates more commercial interest in PTA development.

CRediT authorship contribution statement

Qian Xin: Investigation. **Yufeng Zhao:** Investigation. **Ting Qu:** Investigation. **Chun Zhang:** Methodology. **Yuanfang Huang:** Investigation. **Xiaohai Tang:** Writing – review & editing, Supervision, Conceptualization. **Cheng Zeng:** Investigation. **Huahui Yuan:** Methodology. **Ping Xie:** Project administration. **Zehui Gou:** Writing –

original draft, Investigation. **Sheng-Tao Yang:** Writing – review & editing, Supervision, Funding acquisition, Conceptualization. **Kexin Tang:** Writing – original draft, Investigation. **Guangfu Zeng:** Investigation. **Jinmei Yang:** Investigation.

Declaration of Competing Interest

The authors declare that they have no known competing financial interests or personal relationships that could have appeared to influence the work reported in this paper.

Data availability

Data will be made available on request.

Acknowledgments

Kexin Tang is a student intern from Department of Biology, Emory University. We acknowledge financial support from the Science & Technology Department of Sichuan Province (No. 2023JDRC0014), and the Fundamental Research Funds for the Central Universities, Southwest Minzu University (No. ZYN2022002).

Appendix A. Supporting information

Supplementary data associated with this article can be found in the online version at doi:10.1016/j.colsurfb.2024.113968.

References

[1] W. Wei, X. Zhang, S. Zhang, G. Wei, Z. Su, Biomedical and bioactive engineered nanomaterials for targeted tumor photothermal therapy: a review, Mater. Sci. Eng. C 104 (2019) 109891.
[2] D.-Y. Patil, R. Misra, Rational molecular design towards NIR absorption: efficient diketopyrrolopyrrole derivatives for organic solar cells and photothermal therapy, J. Mater. Chem. C 7 (42) (2019) 13020–13031.
[3] X. Li, J.F. Lovell, J. Yoon, X. Chen, Clinical development and potential of photothermal and photodynamic therapies for cancer, Nat. Rev. Clin. Oncol. 17 (11) (2020) 657–674.
[4] L. Zhao, X. Zhang, X. Wang, X. Guan, W. Zhang, J. Ma, Recent advances in selective photothermal therapy of tumor, J. Nanobiotechnol. 19 (1) (2021) 1–15.
[5] H.S. Jung, P. Verwilst, A. Sharma, J. Shin, J.L. Sessler, J.S. Kim, Organic molecule-based photothermal agents: an expanding photothermal therapy universe, Chem. Soc. Rev. 47 (7) (2018) 2280–2297.
[6] F. Pierini, P. Nakielski, O. Urbanek, S. Pawłowska, M. Lanzi, L. De Sio, T. A. Kowalewski, Polymer-based nanomaterials for photothermal therapy: from light-responsive to multifunctional nanoplatforms for synergistically combined technologies, Biomacromolecules 19 (11) (2018) 4147–4167.
[7] S. Liu, X. Pan, H. Liu, Two-dimensional nanomaterials for photothermal therapy, Angew. Chem. Int. Ed. 59 (15) (2020) 5890–5900.
[8] J. Wang, X. Tan, X. Pang, L. Liu, F. Tan, N. Li, MoS_2 quantum Dot@Polyaniline inorganic-organic nanohybrids for in vivo dual-modal imaging guided synergistic photothermal/radiation therapy, ACS Appl. Mater. Interfaces 8 (37) (2016) 24331–24338.
[9] Y. Xu, S. Long, Y. Yang, F. Zhou, N. Dong, K. Yan, B. Wang, Y. Zeng, N. Du, X. Li, W. R. Chen, Mathematical simulation of temperature distribution in tumor tissue and surrounding healthy tissue treated by laser combined with indocyanine green, Theor. Biol. Med. Model. 16 (1) (2019) 1742–4682.
[10] S. Jeong, H. Liu, W. Chen, Temperature control in deep tumor treatment, Proc. SPIE - Int. Soc. Opt. Eng. (2003).
[11] J.J. Lagendijk, Hyperthermia treatment planning, Phys. Med. Biol. 45 (5) (2000) R61–R76.
[12] M. Luo, L. Shi, F. Zhang, F. Zhou, L. Zhang, B. Wang, P. Wang, Y. Zhang, H. Zhang, D. Yang, G. Zhang, W.R. Chen, X. Wang, Laser immunotherapy for cutaneous squamous cell carcinoma with optimal thermal effects to enhance tumour immunogenicity, Int. J. Hyperther. 34 (8) (2018) 1337–1350.
[13] N. Li, Q. Sun, Z. Yu, X. Gao, W. Pan, X. Wan, B. Tang, Nuclear-targeted photothermal therapy prevents cancer recurrence with near-infrared triggered copper sulfide nanoparticles, ACS Nano 12 (6) (2018) 5197–5206.
[14] X. Dai, X. Li, Y. Du, M. Han, Z. Wang, Y. Wang, F. Yan, Y. Liu, Gold nanorod–mesoporous silica core shell nanocomposites for NIR-II photothermal ablation and dual PD-L1/VEGF blockade therapy in hepatocellular carcinoma, Chem. Eng. J. 459 (2023) 14126.
[15] Y.-Y. Zhao, Z. Chen, L. Zhang, X.-W. Qin, H. Liu, B.-Y. Zheng, M. Ke, J.-D. Huang, X. Li, A self-degradable nanostructured phthalocyanine assembly with high photothermal efficacy to enhanced biosecurity in photothermal therapy, Chem. Eng. J. 474 (2023) 145921.
[16] X. Chang, Q. Wu, Y. Wu, X. Xi, J. Cao, H. Chu, Q. Liu, Y. Li, W. Wu, X. Fang, F. Chen, Multifunctional Au modified Ti_3C_2-MXene for photothermal/enzyme dynamic/immune synergistic therapy, Nano Lett. 22 (20) (2022) 8321–8330.
[17] Y. Zhao, T. Zhao, Y. Cao, J. Sun, Q. Zhou, H. Chen, S. Guo, Y. Wang, Y. Zhen, X. J. Liang, S. Zhang, Temperature-sensitive lipid-coated carbon nanotubes for synergistic photothermal therapy and gene therapy, ACS Nano 15 (4) (2021) 6517–6529.
[18] X. Li, Y. Wang, T. Liu, Y. Zhang, C. Wang, B. Xie, Ultrasmall graphene oxide for combination of enhanced chemotherapy and photothermal therapy of breast cancer, Colloid Surf. B 225 (2023) 113288.
[19] S.S. Lee, F. Oudjedi, A.G. Kirk, M. Paliouras, M.A. Trifiro, Photothermal therapy of papillary thyroid cancer tumor xenografts with targeted thyroid stimulating hormone receptor antibody functionalized multiwalled carbon nanotubes, Cancer Nanotechnol. 14 (1) (2023) 31.
[20] D. Li, K. Huang, J. She, Y. Cai, B. Liu, Z. Wei, Y. Chen, J. Huang, H. Fan, Two-photon fluorescence-guided precise photothermal therapy located in a single cancer cell utilizing bifunctional N-doped carbon quantum dots, J. Colloid Interface Sci. 662 (2024) 719–726.
[21] Z. Wang, X. Zhou, X. Chen, L. Li, T. Wang, W. Zhan, L. Zhang, Wang, C. Wang, Mesoporous carbon nanoparticles embedded with iron in hydrogen-photothermal synergistic therapy, J. Colloid Interface Sci. 663 (2024) 1–8.
[22] J. Gu, J. Wang, X. Nie, W. Wang, J. Shang, Potential role for carbon nanoparticles identification and preservation in situ of parathyroid glands during total thyroidectomy and central compartment node dissection, Int. J. Clin. Exp. Med. 8 (6) (2015) 9640–9648.
[23] C. Yin, X. Wang, S. Sun, Reduction in postoperative hypoparathyroidism following carbon nanoparticle suspension injection combined with parathyroid gland vasculature preservation, J. Int. Med. Res. 48 (1) (2020) 1473–2300.
[24] Y. Huang, G. Zeng, Q. Xin, J. Yang, C. Zeng, K. Tang, S.T. Yang, X. Tang, Carbon nanoparticles suspension injection for photothermal therapy of xenografted human thyroid carcinoma in vivo, MedComm 1 (2) (2020) 202–210.
[25] P. Xie, Y. Huang, K. Tang, X. Wu, C. Zeng, S.-T. Yang, X. Tang, Carbon nanoparticles-Fe(II) complex for efficient theranostics of xenografted colonic tumor, Cancer Nanotechnol. 14 (1) (2023) 1–16.
[26] G.M. Neelgund, A.R. Oki, Influence of carbon nanotubes and graphene nanosheets on photothermal effect of hydroxyapatite, J. Colloid Interface Sci. 484 (2016) 135–145.
[27] L. Chen, C. Wang, S. Yang, X. Guan, Q. Zhang, M. Shi, S.T. Yang, C. Chen, X. L. Chang, Chemical reduction of graphene enhances in vivo translocation and photosynthetic inhibition in pea plants, Environ. Sci. Nano 6 (4) (2019) 1077–1088.
[28] A. Yilihamu, B. Ouyang, P. Ouyang, Y. Bai, Q. Zhang, M. Shi, X. Guan, S.-T. Yang, Interaction between graphene oxide and nitrogen-fixing bacterium *Azotobacter chroococcum*: transformation, toxicity and nitrogen fixation, Carbon 160 (2020) 5–13.
[29] Z. Ming, S. Feng, A. Yilihamu, S. Yang, Q. Ma, H. Yang, Y. Bai, S.T. Yang, Toxicity of carbon nanotubes to white rot fungus *Phanerochaete chrysosporium*, Ecotoxicol. Environ. Saf. 162 (1) (2018) 225–234.
[30] S. Wang, H. Shen, Q. Mao, Q. Tao, G. Yuan, L. Zeng, Z. Chen, Y. Zhang, L. Cheng, J. Zhang, H. Dai, C. Hu, Y. Pan, Y. Li, Macrophage-mediated porous magnetic nanoparticles for multimodal imaging and postoperative photothermal therapy of gliomas, ACS Appl. Mater. Interfaces 13 (48) (2021) 56825–56837.
[31] B. Yang, Y. Zhang, L.J. Wang, Z. Zhao, Z. Huang, W. Mao, R. Xue, R. Chen, J. Luo, T. Wang, J. Jiang, Y. Qin, Modulated ultrasmall γ-Fe_2O_3 nanocrystal assemblies for switchable magnetic resonance imaging and photothermal-ferroptotic-chemical synergistic cancer therapy, Adv. Funct. Mater. 33 (5) (2023) 2211251.
[32] Q. Zhang, Q. Guo, Q. Chen, X. Zhao, S.J. Pennycook, H. Chen, Highly efficient 2D NIR-II photothermal agent with fenton catalytic activity for cancer synergistic photothermal chemodynamic therapy, Adv. Sci. 7 (7) (2020) 1902576.
[33] T. Niemiec, M. Dudek, N. Dziekan, S. Jaworski, A. Przewozik, E. Soszka, A. Koperkiewicz, P. Koczoń, The method of coating Fe_3O_4 with carbon nanoparticles to modify biological properties of oxide measured in vitro, J. AOAC Int. 100 (4) (2017) 905–915.
[34] C. Wu, Z. Shen, Y. Lu, F. Sun, H. Shi, P53 promotes ferroptosis in macrophages treated with Fe_3O_4 nanoparticles, ACS Appl. Mater. Interfaces 14 (38) (2022) 42791–42803.
[35] Y. Liu, X. Zhang, Z. Liu, L. Wang, L. Luo, M. Wang, Q. Wang, D. Gao, Gold nanoshell-based betulinic acid liposomes for synergistic chemo-photothermal therapy, Nanomed. Nanotechnol. 13 (6) (2017) 1891–1900.
[36] G. Jo, E.J. Kim, H. Hyun, Enhanced tumor accumulation of low-molecular-weight hyaluronic acid/chitosan nanocomplexes for photothermal therapy, Pharmaceutics 15 (2) (2023) 1999–4923.
[37] P. He, Q. Lei, B. Yang, T. Shang, J. Shi, Q. Ouyang, W. Wang, L. Xue, F. Kong, Z. Li, J. Huang, L. Liu, J. Guo, C.J. Brinker, K. Liu, W. Zhu, Dual-stage irradiation of size-switchable albumin nanocluster for cascaded tumor enhanced penetration and photothermal therapy, ACS Nano 16 (9) (2022) 13919–13932.
[38] S. Liu, C. Shen, D. Jiang, C. Qian, Z. Yang, J. Wang, W. Ye, Cascade tumor therapy platform for sensitized chemotherapy and penetration enhanced photothermal therapy, Macromol. Biosci. 22 (3) (2022) e2100429.
[39] Z. Yu, W.K. Chan, Y. Zhang, T.T.Y. Tan, Near-infrared-II activated inorganic photothermal nanomedicines, Biomaterials 269 (2021) 120459.
[40] Y. Shi, J. Zhang, H. Huang, C. Cao, J. Yin, W. Xu, W. Wang, X. Song, Y. Zhang, X. Dong, Fe-doped polyoxometalate as acid-aggregated nanoplatform for NIR-II photothermal-enhanced chemodynamic therapy, Adv. Healthc. Mater. 9 (9) (2020) 2192–2640.

[41] L. Zhang, H. Forgham, A. Shen, R. Qiao, B. Guo, Recent advances in single Fe-based nanoagents for photothermal-chemodynamic cancer therapy, Biosensors 12 (2) (2022) 2079–6374.
[42] J. Wu, Q. Wang, X. Dong, M. Xu, J. Yang, X. Yi, B. Chen, X. Dong, Y. Wang, X. Lou, F. Xia, S. Wang, J. Dai, Biocompatible AIEgen/p-glycoprotein siRNA@reduction-sensitive paclitaxel polymeric prodrug nanoparticles for overcoming chemotherapy resistance in ovarian cancer, Theranostics 11 (8) (2021) 3710–3724.
[43] H. Xiong, C. Zhang, L. Han, T. Xu, K. Saeed, J. Han, J. Liu, C.D. Klaassen, F. J. Gonzalez, Y. Lu, Y. Zhang, Suppressed farnesoid X receptor by iron overload in mice and humans potentiates iron-induced hepatotoxicity, Hepatology 76 (2) (2022) 387–403.
[44] M. Tenenbein, Hepatotoxicity in acute iron poisoning, Clin. Toxicol. 39 (7) (2001) 721–726.